arXiv:1606.05607v1 [cond-mat.quant-gas] 17 Jun 2016

Vector Dark-Antidark Solitary Waves in Multi-Component Bose-Einstein condensates

I. Danaila,[1,*] M. A. Khamehchi,[2] V. Gokhroo,[2] P. Engels,[2] and P. G. Kevrekidis[3]

[1]*Laboratoire de Mathématiques Raphaël Salem, Université de Rouen, 76801 Saint-Étienne-du-Rouvray, France*

[2]*Washington State University, Department of Physics & Astronomy, Pullman, WA 99164 USA*

[3]*Department of Mathematics and Statistics, University of Massachusetts Amherst, Amherst, MA 01003-4515, USA*

(Dated: June 20, 2016)

Abstract

Multi-component Bose-Einstein condensates exhibit an intriguing variety of nonlinear structures. In recent theoretical work, the notion of magnetic solitons has been introduced. Here we generalize this concept to vector dark-antidark solitary waves in multi-component Bose-Einstein condensates. We first provide concrete experimental evidence for such states in an atomic BEC and subsequently illustrate the broader concept of these states, which are based on the interplay between miscibility and inter-component repulsion. Armed with this more general conceptual framework, we expand the notion of such states to higher dimensions presenting the possibility of both vortex-antidark states and ring-antidark-ring (dark soliton) states. We perform numerical continuation studies, investigate the existence of these states and examine their stability using the method of Bogolyubov-de Gennes analysis. Dark-antidark and vortex-antidark states are found to be stable for broad parametric regimes. In the case of ring dark solitons, where the single-component ring state is known to be unstable, the vector entity appears to bear a progressively more and more stabilizing role as the inter-component coupling is increased.

PACS numbers:

*Email: ionut.danaila@univ-rouen.fr

I. INTRODUCTION

Atomic Bose-Einstein condensates (BECs) offer an excellent testbed for the exploration of waveforms relevant to multi-component nonlinear wave systems [1, 2]. A principal paradigm consists of the dark-bright (DB) solitary wave and related structures such as dark-dark solitary waves that have long been studied theoretically [3–9]. The experimental study of such states was pioneered much earlier in nonlinear optics, including e.g. the observation of dark-bright solitary wave structures in [10, 11]. Yet, it was the versatility and tunability of BECs that enabled a wide variety of relevant studies initially motivated by the proposal of [12]. Specifically, the experimental realization of DBs [13] was followed by a string of experiments investigating the dynamics and properties of these features including in-trap oscillations of DBs, their spontaneous generation (e.g. via counterflow experiments) and their interactions both with other DBs and with external potential barriers [14–19].

Very recently, a different type of multi-component solitons was proposed, the so-called "magnetic solitons" [20]. Due to the limited number of solitonic families that have been proposed so far, and due to the even fewer number of types observed in experiments, such entities naturally are of great theoretical interest. The ability to generate them using current state-of-the art experiments with multi-component BECs gives them considerable experimental appeal as well. These states have a complementary intensity profile in the two-components $(\psi_1(x,t), \psi_2(x,t))$ and are described by the two-component wave function

$$\begin{pmatrix} \psi_1(x,t) \\ \psi_2(x,t) \end{pmatrix} = \sqrt{n} \begin{pmatrix} \cos(\frac{\theta}{2}) e^{i\phi_1} \\ \sin(\frac{\theta}{2}) e^{i\phi_2} \end{pmatrix}$$

where $\theta(x,t)$ characterizes the spatial distribution of the amplitude, n the total density and ϕ the phase of each component. It is relevant to note that a related idea regarding the ansatz of the multi-component nonlinear wave state was put forth, e.g., in the work of [21].

A complementary possibility recognized considerably earlier was that of dark-antidark solitary waves [22]. Antidark solitary waves are bright solitary waves on top of a finite background. Here, we will avoid calling the structures under investigation "magnetic", as we do not a priori constrain the sum of the densities of the two components to equal that of a single component ground state, as in the settings of [20, 21]. We will show that the idea of complementary non-trivial components, one of which is antidark, is a very general one and is applicable in several dimensions as well: similar ideas naturally emerge in two

dimensions in the form of vortex-antidark and ring-antidark-ring states, which to the best of our understanding have previously not been explored. We motivate and complement our theoretical prediction, numerical verification and stability analysis of such states with an example of an experimental realization in a BEC that confirms that dark-antidark states are straightforward to create and observe the dynamics of in current experimental settings.

The fundamental rationale behind such states is reminiscent of that of the DB entities: For a single-component system, an extensive discussion of the existence and stability of excited states such as dark solitons or vortices can be found in the respective $1d$ and $2d$ chapters of [2]. In a two-component system with inter-component repulsion, a dark soliton or a vortex in one component will induce a potential in the second component. If now atoms of the second ("bright") component are added *in the absence* of a spatially extended background of the second component, the density suppression in the first component will get filled by atoms of the second component and a dark-bright, a vortex-bright [23, 24] or a ring-DB solitary wave [25] will emerge. However, if the second component features a (spatially extended) ground state profile, the presence of inter-component repulsion will produce an effective additional potential which will attract atoms of the second component into the dip of the first one. This generates a bright solitary wave *on top of* the existing nontrivial background, forming an antidark solitary wave. An additional constraint in this case is that the two components need to coexist in the "wings" (i.e., sides) of the dark-antidark (DA), vortex-antidark (VA), or ring-antidark-ring (RAR) structure. This imposes the condition of miscibility between the two species [26–28], i.e. the condition that the inter-component repulsion should be less than the square root of the product of the intra-component ones, $0 \leq g_{12} < \sqrt{g_{11}g_{22}}$. We note in passing here that this condition is derived in the context of homogeneous BECs and is only slightly affected by the presence of weak trapping conditions as in the case examples considered herein [29].

Based on the discussion above, there is a straightforward path that one can follow in order to establish such states (at least, numerically) involving an antidark component. One can start at the uncoupled limit of $g_{12} = 0$ with an excited state (e.g., a dark soliton in $1d$, or a vortex or a ring dark soliton in $2d$) in one component and a fundamental (ground) state in the second component. Then, after turning on the inter-component coupling, the dip of the excited state in the first component will induce an effective attracting potential (due to the inter-component repulsion) in the second component, attracting some atoms into the

dip while maintaining (due to miscibility) the background of the second component. By construction, an antidark structure is formed.

Such a state, as we will see in detail below, will continue to exist for values of g_{12} up to the miscibility-immiscibility threshold. To discuss these types of states, we will proceed as follows: in section II, we will provide an example for an experimental realization of a dark-antidark solitary wave that will serve as a key motivation for the corresponding theoretical more in-depth study. In section III, we will explore the relevant states numerically, using numerical continuation and bifurcation theory, starting from the uncoupled limit described above. Finally, in section IV, we will summarize our conclusions and present some intriguing possibilities for future work.

II. EXPERIMENTAL RESULTS

To motivate our discussion, we begin by presenting experimental evidence for the existence, stability and dynamics of a dark-antidark solitary wave, shown in Fig. 1. In our experiments we observe these features in two-component BECs confined in an elongated dipole trap. The experiments begin by creating a BEC of approximately 0.8×10^6 ^{87}Rb atoms held in an optical trap with harmonic trap frequencies of $\omega_{x,y,z} = 2\pi\{1.4, 176, 174\}$ Hz, where z is the direction of gravity. Evaporation in the dipole trap is continued until no thermal fraction is discernible. Initially, all atoms are in the $|F, m_F\rangle = |1, -1\rangle$ hyperfine state. Subsequently, a brief microwave pulse transfers a fraction of the atoms (approximately 50% for the case shown in Fig. 1) into the $|2, -2\rangle$ hyperfine state. The transfer occurs uniformly across the whole BEC. The resulting two-component BEC can be described by two separate Gross-Pitaevskii equations that are only coupled by the inter-component scattering length (see the theory section below). The intra- and inter-component scattering lengths for the two states are $a_{11} = 100.4a_0$, $a_{22} = 98.98a_0$, and $a_{12} = 98.98a_0$, where a_{11} denotes the scattering of two atoms in the $|1, -1\rangle$ state, a_{12} the scattering between an atom in the $|1, -1\rangle$ and $|2, -2\rangle$ state, and a_{22} between two atoms in the $|2, -2\rangle$ state [30]; a_0 is the Bohr radius. Based on the standard miscibility argument [26–28], discussed above, this mixture is slightly miscible. However, the difference between a_{11} and a_{22} leads to a slight concentration of $|2, -2\rangle$ atoms towards the center of the cloud. When the mixture is held in trap for approximately 10 sec or longer, the emergence of a dark-antidark solitary wave is observed as shown in Fig. 1.

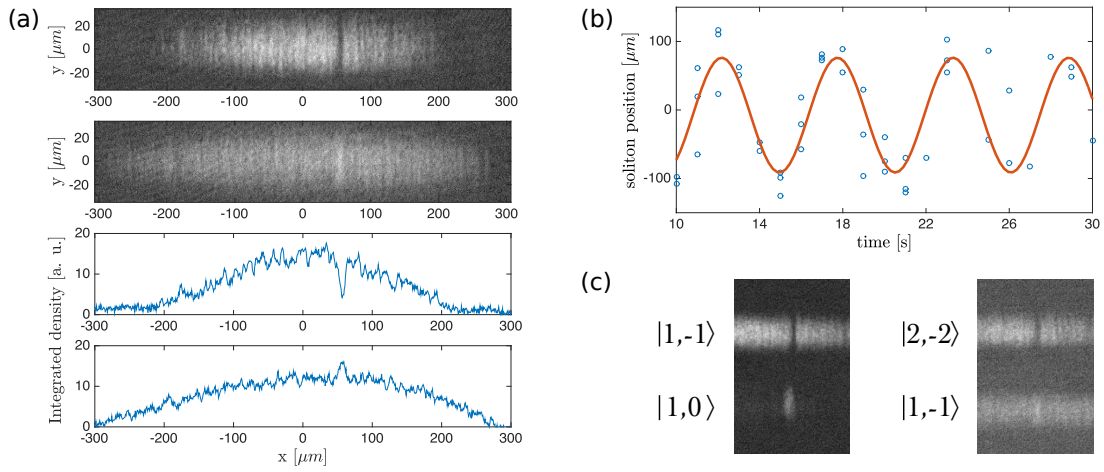

FIG. 1: (Color online) Experimental realization of dark-antidark solitary waves. (a) Absorption images (upper two panels) and corresponding integrated cross sections (lower two panels) of a dark-antidark solitary wave. The dark soliton component resides in a cloud of $|F, m_F\rangle = |2, -2\rangle$ atoms (upper and third panel), while the bright component consists of atoms in the $|F, m_F\rangle = |1, -1\rangle$ state (second and forth panel from top). (b) Experimentally observed oscillation of the dark-antidark solitary wave in the trap. The position is measured along the x-axis, i.e. along the weakly confining axis of the trap. The time is measured starting from the initial microwave pulse that creates the two-component mixture. The blue dots are experimental data, while the red line is a sine function fit to the data. (c) Comparison between a dark-bright soliton in a mixture of atoms in the $|F, m_F\rangle = |1, -1\rangle$ and $|F, m_F\rangle = |1, 0\rangle$ states (left image) and a dark-antidark structure in a mixture of atoms in the $|F, m_F\rangle = |2, -2\rangle$ and $|F, m_F\rangle = |1, -1\rangle$ states (right image).

The solitary waves are imaged by suddenly switching off the trap and imaging the $|2, -2\rangle$ state after 10 ms of expansion and the $|1, -1\rangle$ state after 11 ms of expansion. The difference in the free-fall time separates the two images on the camera, so that the two components appear below each other in the images. During all in-trap evolution leading to the soliton formation, the two components have been well overlapped vertically. Repeating this procedure with well controlled experimental parameters, we observe that each iteration of the experimental run reliably produces a two-component BEC containing one dark-antidark solitary wave such as the one shown in Fig. 1. In all iterations, the dark soliton resides in the $|2, -2\rangle$ component and the antidark soliton is found in the $|1, -1\rangle$ component.

It is remarkable that these features emerge quite "naturally" in our experiments without any dedicated wavefunction engineering [14, 17] or phase imprinting [13]. Furthermore, these features are very long lived. We have observed their in-trap dynamics for up to 30 sec. For comparison, starting with a 50/50 mixture of the two components, we measure the lifetime of the $|2,-2\rangle$ component to be ~ 22 sec and that of $|1,-1\rangle$ component to be ~ 33 sec for our experimental parameters. The emergence of these solitary waves is rather insensitive to the exact mixture ratio of the components. Experimentally we tested and confirmed their existence in a variety of mixtures ranging from 30% of the atoms in the $|2,-2\rangle$ state and 70% in the $|1,-1\rangle$, to mixtures of 50% in the $|2,-2\rangle$ state and 50% in the $|1,-1\rangle$ state. In mixtures where the abundance of the $|2,-2\rangle$ component exceeded approximately 50%, no clear soliton formation was observed.

We have also repeated the experiment with a mixture of atoms in the $|1,-1\rangle$ and $|1,0\rangle$ components. The scattering lengths for this mixture are $a_{11} = 100.4a_0$, $a_{22} = 100.86a_0$, and $a_{12} = 100.41a_0$, where a_{11} now denotes the scattering of two atoms in the $|1,-1\rangle$ state, a_{12} the scattering between an atom in the $|1,-1\rangle$ and $|1,0\rangle$ state, and a_{22} between two atoms in the $|1,0\rangle$ state [30]. This mixture is closer to the miscibility-immiscibility threshold. Following an analogous procedure as described above, no formation of dark-antidark solitary waves was observed. Instead, dark-bright solitons were generated. A comparison between a dark-bright soliton and a dark-antidark one shown in Fig. 1(c), showcasing their very different structure in the bright component. This emphasizes the important role that the miscibility of the component plays for the generation of a non-zero background in the second (bright) component, as has also been highlighted in [20].

The long lifetimes and reproducible generation of dark-antidark solitary waves in a mixture of atoms in the $|2,-2\rangle$ and $|1,-1\rangle$ states allow us to observe their in-trap dynamics (Fig. 1(b)). We clearly detect a slow oscillation of the solitary wave along the weak axis of the trap. A fit of the data in Fig. 1(b) gives an oscillation period of approximately 5.6 sec. For comparison, the period of a dark soliton in a single-component BEC in the same trap is predicted to be 1 sec [31, 32]. Hence, the dark-antidark solitary waves are significantly slower. A similar trend has been found in [12, 15], where it was seen that dark-bright solitons are slowed down when the amount of atoms in the bright component is increased. The theory of "magnetic solitons" described in [20] assumes $a_{11} = a_{22}$, which in our experiment is only approximately fulfilled. This theory predicts an oscillation period on the order of

9.8 sec, somewhat longer than that observed in the experiment. A quantitative comparison between experiment and theory, including the influence of the mixing ratio of the two components and the finite lifetime of the trapped atoms, will be left for future work. Here, these first observations of dark-antidark solitary waves serve as a motivation to investigate (chiefly as a function of the inter-component scattering length) and generalize the underlying concepts of dark-antidark structures using numerical continuation studies and Bogolyubov-de Gennes analysis.

III. THEORETICAL/NUMERICAL RESULTS

In order to capture the qualitative features of the states of interest, it will suffice to utilize a mean-field model in the form of the Gross-Pitaevskii equation. Upon suitable standard reductions [1, 2], the model can be transformed to its dimensionless version in the form:

$$i\frac{\partial \psi_1}{\partial t} = -\frac{1}{2}\Delta\psi_1 + V(\mathbf{x})\psi_1 + \left(g_{11}|\psi_1|^2 + g_{12}|\psi_2|^2\right)\psi_1 \tag{1}$$

$$i\frac{\partial \psi_2}{\partial t} = -\frac{1}{2}\Delta\psi_2 + V(\mathbf{x})\psi_2 + \left(g_{12}|\psi_1|^2 + g_{22}|\psi_2|^2\right)\psi_2 \tag{2}$$

Here, the pseudo-spinor field is denoted by $(\psi_1, \psi_2)^T$ (where ^{T} is used for transpose), $V(\mathbf{x}) = \frac{\Omega^2}{2}\mathbf{x}^2$ represents the parabolic trap, while g_{ij} are the interaction coefficients, proportional to the experimental scattering lengths mentioned above. In line with the analysis of [20], we will assume in what follows that $g_{11} = g_{22} = g$, while $0 \leq g_{12} \leq g$. Given that only the ratios of the scattering lengths matter, we will choose $g = 1$, while $0 \leq g_{12} < 1$, in order to be in the miscible regime, while preserving inter-component repulsion.

In our numerics, the stationary states $(\psi_1^{(0)}, \psi_2^{(0)})^T$ are identified by virtue of a fixed point iteration (typically a Newton method) originally at $g_{12} = 0$, i.e., the limit where the two components are uncoupled. Then, parametric continuation is utilized in order to follow the configuration as a function of g_{12} up to the miscibility threshold.

Upon computing the solution, Bogolyubov-de Gennes stability analysis is implemented that perturbs the solutions according to:

$$\psi_1 = e^{-i\mu_1 t}\left(\psi_1^{(0)}(\mathbf{x}) + \delta(a(\mathbf{x})e^{i\omega t} + b^\star(\mathbf{x})e^{-i\omega^\star t})\right) \tag{3}$$

$$\psi_2 = e^{-i\mu_2 t}\left(\psi_2^{(0)}(\mathbf{x}) + \delta(c(\mathbf{x})e^{i\omega t} + d^\star(\mathbf{x})e^{-i\omega^\star t})\right) \tag{4}$$

Here ω represents the linearization eigenfrequency and the vector $(a, b, c, d)^T$ is the linearized eigenvector pertaining to the respective eigenfrequency. The chemical potentials are denoted by (μ_1, μ_2), while δ is a formal small parameter of the linearization ansatz. Ω represents the strength of the trapping potential in the longitudinal vs. the transverse directions (i.e., the ratio thereof) and thus needs to be $\Omega \ll 1$ for the reductions to be meaningful. In the following we will assume $\Omega = 0.2$ and $\mu_1 = \mu_2 = 2$ unless noted otherwise.

Numerical computations are performed using FreeFem++ [33]. The numerical system developed for computing stationary solutions of the Gross-Pitaevskii equation [34] was extended for the two-component system (1)-(2). We use quadratic (P^2) finite elements with mesh adaptivity, offering high-resolution of the steep gradients in the solution. The Bogolyubov-de Gennes linear eigenvalue problem corresponding to the P^2 finite element discretization is solved using the ARPACK library.

A. 1d: Dark-Antidark Solitary Waves

We start by considering the scenario of dark-antidark solitons in one spatial dimension. Solutions of this type are represented in Fig. 2.

For $g_{12} = 0$ the solution has the form of a regular dark solitary wave coupled to a fundamental state in the second component. For a finite value of g_{12} the stationary solution develops a bump at the location of the dark soliton dip. Due to the inter-component repulsion, the density dip in the the first component leads to an attracting potential well for the second component. Therefore an antidark peak is formed that becomes stronger as g_{12} is increased, while the first component tends to vanish as the miscibility-immiscibility threshold of $g_{12} = 1$ is approached. This trend is clearly seen in the top panel of Fig. 2. For this case, we have used $\Omega = 0.025$, although similar results have been found for other values of the trap strength.

Remarkably, in the case of the dark-antidark solitary wave family we find the relevant solution to be generally stable (as shown in the right panel of Fig. 2) through a wide interval of variation of the g_{12} parameter; an extremely weak oscillatory instability arises for $0.71 < g_{12} < 0.87$, that will be discussed further below, yet its growth rate is so small that we do not expect it to affect the dynamics in an observable way over the time scales of interest. In the large chemical potential limit, we in fact have a detailed handle on the spectrum of

the relevant eigenfrequencies in an analytical form. When $g_{12} = 0$, the second component is uncoupled from the first and its spectrum in the ground state consists of eigenfrequencies

$$\omega = \sqrt{\frac{n(n+1)}{2}}\Omega \tag{5}$$

where n is a non-negative integer, as discussed in [35, 36]. The dark soliton (DS) spectrum on the other hand, as explained, e.g., in [2] consists of the spectrum of the ground state in which the soliton is "embedded", given by Eq. (5), as well as an extensively studied anomalous (or negative energy) mode associated structurally with the excited state nature of the DS state, and practically with its oscillation inside the parabolic trap. As is well known, the latter mode has the frequency $\omega = \Omega/\sqrt{2}$ in the large chemical potential limit [31, 32] and is the lowest excitation frequency in the system. Using an argument similar to that presented in [20], we expect that the relevant mode scales as $\omega \approx \Omega\sqrt{\delta g/(2g)}$, where $\delta g = g - g_{12}$. This prediction is also represented in the right panel of Fig. 2 and is in reasonable agreement with the corresponding numerical result throughout the interval of variation of g_{12}. Regarding the rest of the spectrum (the modes associated with the ground state in each component), it can be seen that they can be partitioned into two fundamental categories, namely those that are essentially left invariant and those that undergo a rapid monotonic decrease (which is nearly linear for small g_{12}) as g_{12} increases. As this takes place, it is in principle possible for the anomalous mode (of dark soliton oscillation) and the lowest frequency associated with the ground state to collide and lead to a resonant eigenfrequency quartet [2]. This does happen in the example of Fig. 2 for $0.71 < g_{12} < 0.87$, yet as mentioned above the growth rate of this instability is miniscule and hence it will not be considered further herein.

B. 2d: Vortex-Antidark Solitary Waves

We now generalize the above concept to the 2d case, as is shown in Fig. 3. Our first example in this setting replaces the 1d dark soliton by a 2d vortex in the first component that generates an attractive potential well for the second component. Once again, it can be seen that starting from the decoupled limit of $g_{12} = 0$ and increasing g_{12} in the miscible regime, the coupled vortex-antidark state emerges with progressively more and more atoms of the second component being radially concentrated in the well formed by the vortex. This creates a radially symmetric antidark solitary wave in the second component.

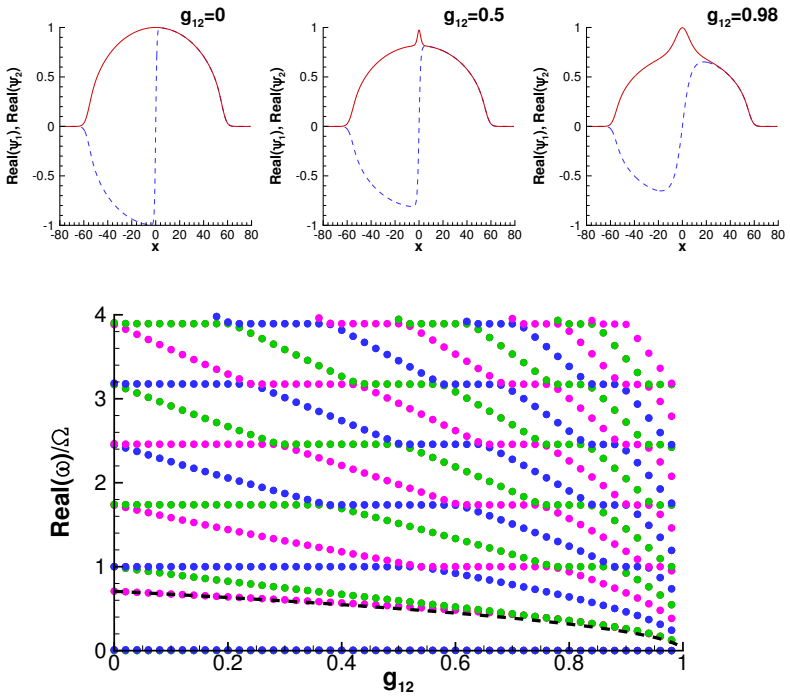

FIG. 2: (Color online) The top panel of the figure shows 3 examples of the two components in the dark-antidark state for progressively increasing g_{12}, i.e., for $g_{12} = 0$, $g_{12} = 0.5$, and for $g_{12} = 0.98$ The bottom panel shows the dependence of the lowest eigenfrequencies scaled by the trap frequency Ω which in this 1d example is chosen to be $\Omega = 0.025 \ll 1$. The dashed black line indicates the theoretical prediction for the anomalous mode (see discussion in the text). The colors in the bottom panel are there only to visually aid the eye to identify the continuation of the different modes.

For this case, the spectrum is shown in the bottom right panel of the figure and also features two sets of constituents. In the limit of $g_{12} = 0$, the ground state component consists of frequencies theoretically approximated (in the Thomas-Fermi limit of large μ considered here) by

$$\omega = \sqrt{m + 2k(1+m) + 2k^2}\Omega, \tag{6}$$

where $k, m \geq 0$ are non-negative integers. The first component bearing the vortex also shares these frequencies (due to the vortex being again "embedded" within the ground state), but additionally carries an anomalous (negative energy) mode that is a signature of its excited state nature [2]. This mode is associated with the rotation of the vortex around the center of the parabolic trap. It is well characterized by the frequency $\omega = \frac{\Omega^2}{2\mu}\log(A\mu/\Omega)$,

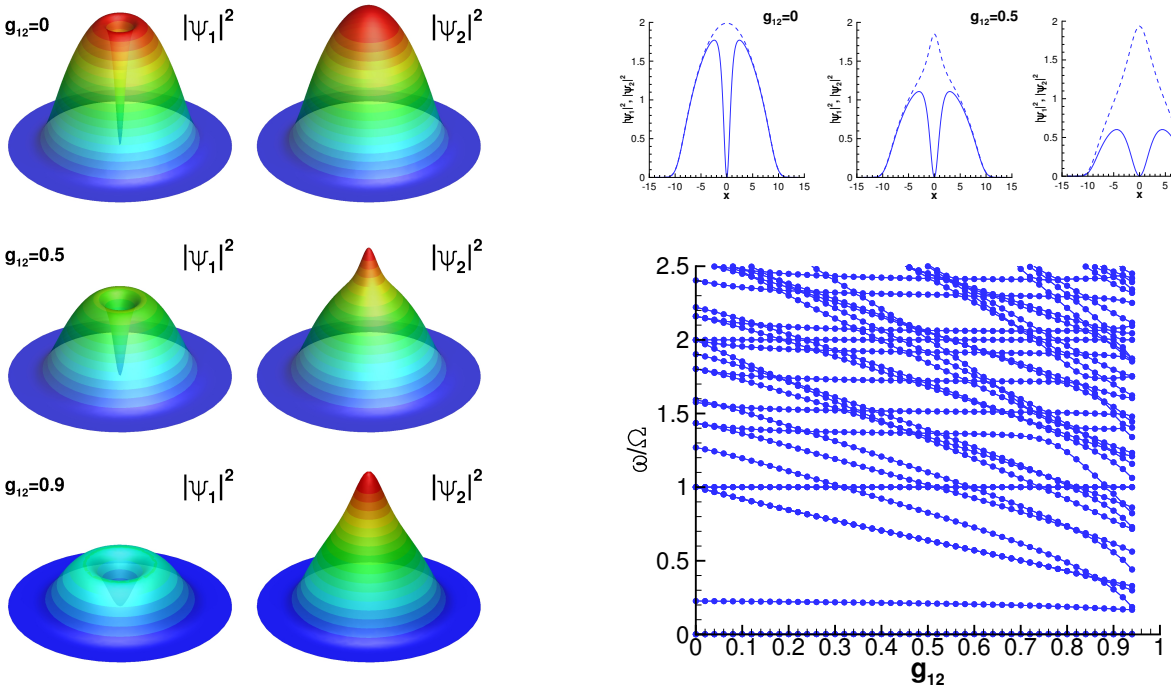

FIG. 3: (Color online) In the left panels of the figure, we see three-dimensional renderings of the density as a function of $x-y$ for the vortex-antidark states and for the particular values of $g_{12}=0$, 0.5 and 0.9. The top right panel illustrates for completeness a cut through the density of these states (at $y=0$). Lastly, the bottom right panel illustrates how the frequencies of the spectral BdG analysis "evolve" as g_{12} is varied (see also the relevant detailed discussion in the text). Notice that all frequencies remain real over the parametric interval considered, indicating the spectral stability/dynamical robustness of the associated state.

where $A \approx 2\sqrt{2}\pi$ [37]. As g_{12} is increased, a similar trend as in 1d is observed: one set of frequencies remains invariant, while a second set, originally degenerate with the first at g_{12}=0, monotonically decreases as $\delta g \to 0$. The anomalous mode frequency associated with the vortex monotonically decreases as well, although in a less pronounced manner.

Physically, this implies that the additional atoms stored within the antidark component decrease the rotation frequency (i.e., increase the rotation period) of the composite entity within the trap. A similar behavior was found for dark-bright solitons even experimentally [12, 15]. Thus, for dark-antidark solitons and for vortex-antidark solitary waves, "heavier means slower".

C. 2d: Ring-Antidark-Ring Solitary Waves

Finally, to illustrate the generality of the underlying concept, we explore the role of increasing the inter-component (repulsive) coupling g_{12} in the miscible regime for the case where the first component bears a ring dark soliton (RDS), while the second one is started in the ground state, again at large μ (i.e., in the vicinity of the Thomas-Fermi limit). Ring dark solitons have been predicted early on in the context of BECs [38], following their proposal and even experimental observation in nonlinear optics [39, 40]. Subsequent detailed studies of their stability [41, 42] illustrated that they are unstable for all values of the chemical potential from the linear limit onwards, progressively becoming more unstable as μ is increased. The initial instability is towards a quadrupolar mode leading to 4 vortices, while subsequently hexapolar (leading to 6 vortices), octapolar (leading to 8 vortices) etc. instabilities arise in the relevant spectrum.

Here, we observe the relevant states in Fig. 4. A progressive increase of g_{12} generates an attractive annular potential for atoms in the second component so that an antidark ring is formed in the second component. As with the previous states, the increase of g_{12} also decreases the density of the dark ring component (for the same chemical potential), finally leading it towards extinction as the miscibility-immiscibility threshold is approached. An associated and quite interesting feature is that as g_{12} is increased, progressively more and more unstable modes of the original single component RDS are *stabilized*, hence it is intriguing to note that for the same chemical potential states with larger g_{12} and hence larger antidark component are less susceptible to instability. In fact, the state tends towards complete stabilization as the miscibility threshold is approached, a feature inter-related with the tendency towards extinction of the associated RDS component. It is relevant to note also that in these last two cases (of Figs. 3 and 4) the state appears to terminate *noticeably before* the homogeneous miscibility limit of $g_{12} = 1$, while the 1d corresponding state can be identified continuously up to the miscibility-immiscibility threshold.

IV. CONCLUSIONS & FUTURE WORK

In the present paper, we propose a multitude of states motivated by the recent proposal of magnetic solitons put forth in [20]. These "dark-antidark" states that we discuss are based

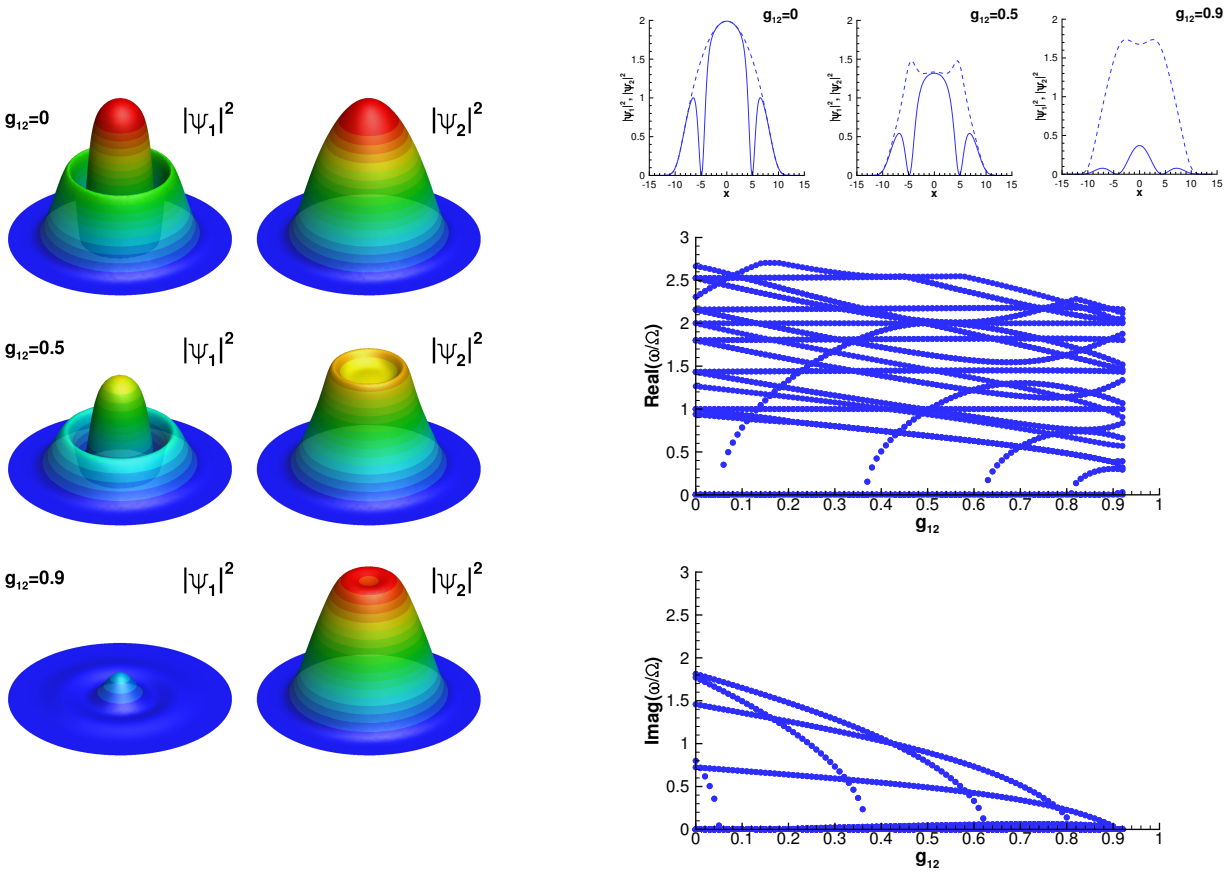

FIG. 4: (Color online) Same as the previous figure, but now for the dark-antidark ring state. The left panel presents the 3d profiles of the state and the top right illustrates the cross sections (for $y = 0$). The bottom right panel shows the real and imaginary parts of the linearization eigenfrequencies of the system normalized by the trap frequency of $\Omega = 0.2$. Notice how the imaginary eigenfrequencies associated with instabilities to (azimuthal) snaking progressively disappear as g_{12} is increased. I.e., the ring antidark solitary wave has a stabilizing effect on the unstable ring dark soliton.

on a simple physical principle, namely the formation of an attractive potential well on top of a ground state component by the presence of a "dark" structure in the other component. In the miscible case with inter-component repulsion, this potential well attracts atoms and forms an antidark entity (a 1d soliton, a 2d soliton or even a ring soliton) in the (formerly) ground state component. This is a natural generalization also of the notion of dark-bright solitons which have recently been extensively explored.

We have proposed this notion at an intuitive/theoretical level and have illustrated its generality via detailed numerical computations. Furthermore, we have showcased it in ex-

periments, at least in as far as its 1d installment is concerned. This emphasizes the relevance of these features for current experiments with multi-component BECs. An additional appealing feature of such symbiotic structures lies in the fact that when the single component entity (such as the ring dark soliton) may be unstable, this coupling appears to have a stabilizing effect rendering the relevant entity more amenable to observation. Both the existence and the spectral stability characteristics of these states were explained over variations of the inter-component coupling throughout their range of existence.

Naturally, there are many open directions for future study in this subject. From an experimental perspective, it would be particularly interesting to explore the possibility to form such states in both two- and three-dimensions. In the latter setting of 3d, computations would also be especially useful in elucidating such states: recently, vortex-line-bright and vortex-ring-bright [43] states have been identified, and their generalization to antidark ones would be quite relevant, as well as the study of their stability. From a theoretical perspective, it would also be quite intriguing to explore further the "particle description" of such entities, both at the level of the single particle (e.g. characterizing the rotation of a vortex-antidark solitary wave etc.), but also quite importantly at the level of interaction of multiple such entities. The latter has not been quantified even in 1d settings. As a final but important point, we note the sensitive dependence of the emergence in experiments of the dark-antidark vs. dark-bright solitons on the value of scattering lengths in the vicinity of the miscibility threshold. This is a feature worth further elucidating in future experiments and corresponding theoretical analyses. Some of these topics are presently under consideration and will be reported in future publications.

Acknowledgments

P.G.K. gratefully acknowledges the support of NSF-DMS- 1312856, and the ERC under FP7, Marie Curie Actions, People, International Research Staff Exchange Scheme (IRSES-605096). He also acknowledges the warm hospitality of the Laboratoire de Mathématiques Raphaël Salem at the University of Rouen. P.E. gratefully acknowledges funding from NSF under grant number PHY-1306662. ID acknowledges support from the French ANR grant

ANR-12-MONU-0007-01 BECASIM (Modéles Numériques call).

---

[1] L. P. Pitaevskii and S. Stringari, *Bose-Einstein Condensation.* Oxford University Press (Oxford, 2003).

[2] P. G. Kevrekidis, D. J. Frantzeskakis, and R. Carretero-González, *The Defocusing Nonlinear Schrödinger Equation*, SIAM (Philadelphia, 2015).

[3] D. N. Christodoulides, Phys. Lett. A, **132**, 451–452 (1988).

[4] V. V. Afanasyev, Yu. S. Kivshar, V. V. Konotop, and V. N. Serkin, Opt. Lett., **14**, 805–807 (1989).

[5] Yu. S. Kivshar and S. K. Turitsyn, Opt. Lett., **18**, 337–339 (1993).

[6] R. Radhakrishnan and M. Lakshmanan, J. Phys. A: Math. Gen., **28**, 2683–2692 (1995).

[7] A. V. Buryak, Yu. S. Kivshar, and D. F. Parker, Phys. Lett. A, **215**, 57–62 (1996).

[8] A. P. Sheppard and Yu. S. Kivshar, Phys. Rev. E, **55**, 4773–4782 (1997).

[9] Q.-H. Park and H. J. Shin, Phys. Rev. E, **61**, 3093–3106 (2000).

[10] Z. Chen, M. Segev, T. H. Coskun, D. N. Christodoulides, and Yu. S. Kivshar, J. Opt. Soc. Am. B, **14**, 3066–3077 (1997).

[11] E. A. Ostrovskaya, Yu. S. Kivshar, Z. Chen, and M. Segev, Opt. Lett., **24**, 327–329 (1999).

[12] Th. Busch and J. R. Anglin, Phys. Rev. Lett., **87**, 010401 (2001).

[13] C. Becker, S. Stellmer, P. Soltan-Panahi, S. Dörscher, M. Baumert, E.-M. Richter, J. Kronjäger, K. Bongs, and K. Sengstock, Nature Phys., **4**, 496–501 (2008).

[14] C. Hamner, J. J. Chang, P. Engels, and M. A. Hoefer, Phys. Rev. Lett., **106**, 065302 (2011).

[15] S. Middelkamp, J. J. Chang, C. Hamner, R. Carretero-González, P. G. Kevrekidis, V. Achilleos, D. J. Frantzeskakis, P. Schmelcher,and P. Engels, Phys. Lett. A, **375**, 642–646 (2011).

[16] D. Yan, J. J. Chang, C. Hamner, P. G. Kevrekidis, P. Engels, V. Achilleos, D. J. Frantzeskakis, R. Carretero-González, and P. Schmelcher, Phys. Rev. A, **84**, 053630 (2011).

[17] M. A. Hoefer, J. J. Chang, C. Hamner, and P. Engels, Phys. Rev. A, **84**, 041605(R) (2011).

[18] D. Yan, J. J. Chang, C. Hamner, M. Hoefer, P. G. Kevrekidis, P. Engels, V. Achilleos, D. J. Frantzeskakis, and J. Cuevas, J. Phys. B: At. Mol. Opt. Phys., **45**, 115301 (2012).

[19] A. Álvarez, J. Cuevas, F. R. Romero, C. Hamner, J. J. Chang, P. Engels, P. G. Kevrekidis,

and D. J. Frantzeskakis, J. Phys. B, **46**, 065302 (2013).

[20] C. Qu, L.P. Pitaevskii and S. Stringari, Phys. Rev. Lett. **116**, 160402 (2016).

[21] A.L. Fetter, Phys. Rev. A **89**, 023629 (2014); see in particular Eq. (17) for the relevant ansatz.

[22] P.G. Kevrekidis, H.E. Nistazakis, D.J. Frantzeskakis, B.A. Malomed and R. Carretero-González, Eur. Phys. J. D **28**, 181 (2004).

[23] K. J. H. Law, P. G. Kevrekidis, and L. S. Tuckerman, Phys. Rev. Lett., **105**, 160405 (2010).

[24] M. Pola, J. Stockhofe, P. Schmelcher, and P. G. Kevrekidis, Phys. Rev. A, **86**, 053601 (2012).

[25] J. Stockhofe, P.G. Kevrekidis, D.J. Frantzeskakis, P. Schmelcher, J. Phys. B At. Mol. Opt. Phys. **44**, 191003 (2011).

[26] E. Timmermans, Phys. Rev. Lett. 81, 5718 (1998);

[27] H. Pu and N. P. Bigelow, Phys. Rev. Lett. **80**, 1130 (1998)]

[28] P. Ao and S. T. Chui Phys. Rev. A **58**, 4836 (1998).

[29] R. Navarro, R. Carretero-González, and P. G. Kevrekidis Phys. Rev. A **80**, 023613 (2009).

[30] Servaas Kokkelmans, private communication; B. J. Verhaar, E.G.M. van Kempen, and S.J.J.M.F. Kokkelmans, Phys. Rev. A **79**, 032711 (2009).

[31] Th. Busch and J. R. Anglin, Phys. Rev. Lett., **84**, 2298 (2000).

[32] V. V. Konotop and L. Pitaevskii, Phys. Rev. Lett., **93**, 240403 (2004).

[33] F. Hecht, Journal of Numerical Mathematics **20**, 251 (2012).

[34] I. Danaila, F. Hecht, J. Comput. Physics **229**, 6946 (2010).

[35] S. Stringari, Phys. Rev. Lett. **77**, 2360 (1996).

[36] P.G. Kevrekidis and D.E. Pelinovsky, Phys. Rev. A **81**, 023627 (2010).

[37] S. Middelkamp, P.G. Kevrekidis, D.J. Frantzeskakis, R. Carretero-González, and P. Schmelcher, Phys. Rev. A **82**, 013646 (2010).

[38] G. Theocharis, D. J. Frantzeskakis, P. G. Kevrekidis, B. A. Malomed, and Yu.S. Kivshar Phys. Rev. Lett. **90**, 120403 (2003)

[39] Yu.S. Kivshar and X. Yang, Phys. Rev. E **50**, R40 (1994).

[40] D. Neshev, A. Dreischuh, V. Kamenov, I. Stefanov, S. Dinev, W. Fliesser, and L. Windholz, Appl. Phys. B **64**, 429 (1997); A. Dreischuh, D. Neshev, G. G. Paulus, F. Grasbon, and H. Walther, Phys. Rev. E **66**, 066611 (2002).

[41] G. Herring, L.D. Carr, R. Carretero-González, P.G. Kevrekidis, D.J. Frantzeskakis, Phys. Rev. A **77**, 023625 (2008).

[42] S. Middelkamp, P.G. Kevrekidis, D.J. Frantzeskakis, R. Carretero-González, P. Schmelcher, Physica D **240**, 1449 (2011).

[43] E. G. Charalampidis, W. Wang, P. G. Kevrekidis, D. J. Frantzeskakis, J. Cuevas-Maraver, arXiv:1604.04690.